System-Level Performance of Limited Feedback Schemes for Massive MIMO

Yongin Choi, Jaewon Lee, Minjoong Rim, Chung Gu Kang, Junyoung Nam, and Young-Jo Ko

To implement high-order multiuser multiple input and multiple output (MU-MIMO) for massive MIMO systems, there must be a feedback scheme that can warrant its performance with a limited signaling overhead. The interference-to-noise ratio can be a basis for a novel form of Codebook (CB)-based MU-MIMO feedback scheme. The objective of this paper is to verify such a scheme's performance under a practical system configuration with a 3D channel model in various radio environments. We evaluate the performance of various CB-based feedback schemes with different types of overhead reduction approaches, providing an experimental ground with which to optimize a CB-based MU-MIMO feedback scheme while identifying the design constraints for a massive MIMO system.

Keywords: Massive MIMO, FD-MIMO, 3D-channel model, codebook-based feedback, system level simulation, interference-to-noise ratio, multiuser interference indicator, MUI, INR.

Manuscript received Mar. 4, 2015; revised Nov. 17, 2015; accepted Nov. 26, 2015.

This work was supported by the ICT R&D program of MSIP/IITP (14-000-04-001, Development of 5G Mobile Communication Technologies for Hyper-connected Smart Services).

Yongin Choi (only1korea@korea.ac.kr), Jaewon Lee (lijrew@korea.ac.kr), and Chung Gu Kang (corresponding author, ccgkang@korea.ac.kr) are with the School of Electrical Engineering, Korea University, Seoul, Rep. of Korea.

Minjoong Rim (minjoong@dongguk.edu) is with the Department of Information and Communication Engineering, Dongguk University, Seoul, Rep. of Korea.

Junyoung Nam (jynam@etri.re.kr) and Young-Jo Ko (koyj@etri.re.kr) are with the 5G Giga Communication Research Laboratory, ETRI, Daejeon, Rep. of Korea.

I. Introduction

A key technology in next-generation mobile communication systems is that of massive multiple input and multiple output (MIMO) or full-dimension (FD)-MIMO, where a base station or an evolved Node B (eNB) with a very large number of antenna elements serves a large number of user equipments (UEs) simultaneously on the same time-frequency resource set [1]–[3]. For downlink transmissions in a massive MIMO system, an eNB requires downlink channel state information (CSI) to perform beamforming for multiple UEs and to effectively nullify inter-user interference. When time-division duplexing (TDD) is employed, downlink CSI can be extracted from uplink signals using the channel reciprocity. However, since frequency-division duplexing (FDD) is used in most existing cellular systems, effective CSI feedback schemes need to be developed to minimize the feedback overhead while maintaining high system throughputs [4]–[12].

To reduce feedback overhead, a massive MIMO system can use a finite set of precoding matrices, called a codebook (CB). When only one UE is served each time with a CB-based feedback scheme, a feedback of a single CB index is sufficient for beamforming. In a multiuser MIMO (MU-MIMO) system in which multiple UEs are simultaneously scheduled on the same time-frequency resource, however, multiple CB indices that minimize the multiuser interference must be reported so as to avoid performance degradation due to interference. In [13], a novel CB-based MU-MIMO feedback scheme was proposed by employing a feedback of interference-to-noise ratio (INR) for a given codebook. This scheme, referred to as a multiuser interference indicator (MUI) feedback scheme in this paper, allows an eNB to perform high-order MU-MIMO with flexible scheduling while reducing feedback overhead as well as

dedicated pilot overhead. Some simulation results are also provided in [13] based on a one-ring channel model to show that high-order MU-MIMO is feasible in FDD-based massive MIMO systems. Although the simulation results in [13] are very satisfactory, they are not acceptable for realistic cellular systems, since it is critical to evaluate the performance of such systems under a more detailed system-level simulation (SLS) setup, including cell structures, scheduling, and a practical 3D channel model to capture the channel features of a massive MIMO system. It would be possible to extract insights from the simulation results for performance improvement or overhead reduction only with the SLS results under realistic environments.

In this paper, we present system performance results for an MUI scheme with SLS. In the SLS, we consider FD-MIMO scenarios with a 2D-active antenna array system (AAS), which are described in the 3rd Generation Partnership Project (3GPP) [14]. The SLS, including the 3D channel model, is verified with calibration procedures specified in [14] and [15]. We also discuss the characteristics of high-order MU-MIMO in massive MIMO systems using various SLS results with different antenna configurations — for example, antenna polarization; number of horizontal antenna elements; and different cellular environments — for example, urban macro (UMa) or urban micro (UMi).

The rest of this paper is organized as follows. Section II describes the system model considered in this paper, including antenna configurations, CBs, scheduling, and several MU-MIMO feedback schemes, including MUI. The system-level evaluation results of the MU-MIMO feedback schemes are given in Section III, and a further analysis based on the simulation results is provided in Section IV. Finally, conclusions are drawn in Section V.

II. System Model

1. Massive MIMO System Model

A. Antenna Configuration

In this paper, a uniformly spaced 2D planar antenna array model is used. Its configuration is represented by (M, N, P), where M is the number of antenna elements with the same polarization in each column, N is the number of columns, and P is the number of polarization dimensions. Figures 1(a) and 1(b) illustrate an antenna configuration for (M, N, 2) and (M, N, 1), respectively. We consider a UE antenna configuration of (1, 1, 2) with a cross polarization (X-pol) of 0° and 90°; eNB has various antenna configurations with either a uniform linear array (ULA) or X-pol of ±45° [14], [15]. In the current evaluation, we consider a total of 64 antennas; for example, M = 8, N = 4, and P = 2 for the configuration in Fig. 1(a), which is considered as a realizable case of massive MIMO in practice, as implied in [14] and [15].

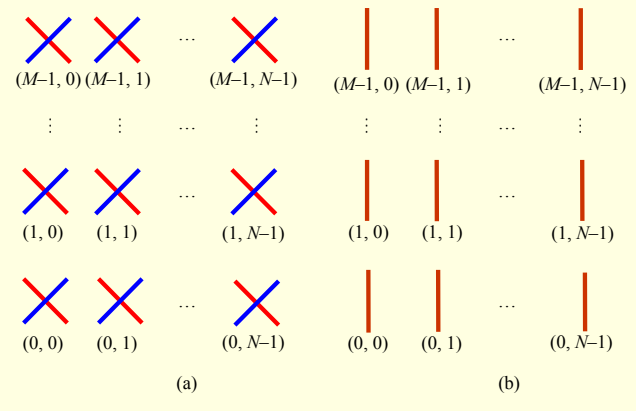

Fig. 1. 2D planar antenna structure with (a) X-pol and (b) ULA.

B. Codebook for MU-MIMO

A rank-1 CB, denoted by $\mathcal{W}$, is employed for MU-MIMO, in which a single data layer is assigned to each UE i by a beamforming vector $\mathbf{w}_i \in \mathcal{W}$. Note that for a rank-1 CB, we consider an oversampled discrete Fourier transform (DFT) beamforming vector, which is defined by an ordered pair (i_1, i_2) for UE i.

A baseline vector $\mathbf{c}_\ell$ defined as

$$\mathbf{c}_\ell = \frac{1}{\sqrt{N}}\left[1, e^{-\mathrm{j}2\pi\cdot\frac{\ell}{2N}}, \ldots, e^{-\mathrm{j}2\pi\cdot\frac{(N-1)\ell}{2N}}\right]. \quad (1)$$

For P = 1, we have a ULA-based CB with beamforming vectors $\mathbf{w}_i = \mathbf{c}^{\mathrm{T}}_{2i_2+i_1}$ (i_1 = 0, 1 and i_2 = 0, 1, … , N – 1). For P = 2 (that is, X-pol), we consider a double CB (a subsampled version of beamforming vector $\mathbf{w}_i$), which is given as $\mathbf{w}_i = [\mathbf{c}_{i_2} \;\; a_{i_1}\mathbf{c}_{i_2}]^{\mathrm{T}}$ (i_1 = 0, 1 and i_2 = 0, 1, … , 2N – 1), where $a_{i_1} \in \{1, -1\}$. Let $\mathcal{C}$ denote a set of codebook indices; that is, $\mathcal{C} = \{1, 2, \ldots, |\mathcal{W}|\}$. Note that each beamforming vector has a dimension of PN; And there exist 2PN beamforming vectors (that is, $|\mathcal{W}| = 2PN$).

C. MU-MIMO System Model

Each eNB employs a 2D AAS (M, N, P); that is, a total of $N_{\mathrm{T}} = M \times N \times P$ transmit antennas. The antenna configuration of all UEs is (1, 1, 2); that is, a total of $N_{\mathrm{R}} = 1 \times 1 \times 2$ receive antennas. Meanwhile, a fixed tilting is considered in the vertical dimension for the 3D channel model [16]. Denoting an effective channel with all Tx/Rx antennas and vertical tilting by $\tilde{\mathbf{H}}$, the signal received by the UE for an MU-MIMO scenario is given as

$$\mathbf{y} = \tilde{\mathbf{H}}\mathbf{x} + \mathbf{n}, \tag{2}$$

where $\mathbf{x}$ is an input signal vector, $\mathbf{x} = [x_1, x_2, \ldots, x_K]^{\mathrm{T}}$, of rank K, of the input covariance given by $\sum = \mathrm{E}[\mathbf{x}\mathbf{x}^{\mathrm{H}}]$, and $\mathbf{n}$ denotes Gaussian noise including other-cell interference with an average power of σ_n^2, in a multicell environment.

Let $\mathcal{S}$ denote a set of UEs that are scheduled for MU-MIMO transmission (that is, $|\mathcal{S}| = K$). Furthermore, let $\mathbf{w}_u \in \mathcal{W}$ and d_u, u denotes a UE ($u = 1, \ldots, K$, $u \in \mathcal{S}$), denote a beamforming vector and a data symbol for a UE, respectively. We consider a single data stream per user. Assuming an equal power allocation to all users served by the given eNB with transmit power of ρ; that is, $\mathrm{tr}(\sum) = \rho/K \cdot \mathbf{I}_K$, the received signal for a UE is given as

$$\mathbf{y}_u = \sqrt{\rho/K} \cdot (\tilde{\mathbf{H}}_u \mathbf{w}_u d_u + \textstyle\sum_{j \in \mathcal{S} \setminus u} \tilde{\mathbf{H}}_u \mathbf{w}_j d_j) + \mathbf{n}. \tag{3}$$

Furthermore, its signal-to-interference-plus-noise ratio (SINR) is represented as

$$\gamma_u = \frac{\left|\mathbf{g}_u \tilde{\mathbf{H}}_u \mathbf{w}_u\right|^2}{K\sigma_u^2 + \left\|\mathbf{g}_u \tilde{\mathbf{H}}_u \mathbf{W}_{-u}\right\|_{\mathrm{F}}^2}, \tag{4}$$

where $\sigma_u^2 = |\mathbf{g}_u|^2 \sigma_n^2/\rho$, $\mathbf{W}_{-u}$ denotes a precoding matrix that excludes the uth precoding vector (that is, $\mathbf{W}_{-u} = [\mathbf{w}_1, \ldots, \mathbf{w}_{u-1}, \mathbf{w}_{u+1}, \ldots, \mathbf{w}_K]$) and $\mathbf{g}_u$ is a minimum mean square error-interference rejection combining (MMSE-IRC) filter in the receiver, which is given as

$$\mathbf{g}_u = \left(\tilde{\mathbf{H}}_u \mathbf{w}_u\right)^{\mathrm{H}} \left(\frac{\rho}{K} \tilde{\mathbf{H}}_u \mathbf{w}_u \left(\tilde{\mathbf{H}}_u \mathbf{w}_u\right)^{\mathrm{H}} + \sigma_n^2 \mathbf{I}_{N_R}\right)^{-1}. \tag{5}$$

D. Scheduling

Based on the precoding matrix indicator (PMI) information and the channel quality information (CQI) from UEs, eNB determines a set of users that will be scheduled for MU-MIMO transmission (see Fig. 2). The scheduling is performed every time slot t and the number of scheduled users, denoted as K, varies from 1 to $K_{\max}$; that is, $K \in \{1, 2, \ldots, K_{\max}\}$. Let $\mathcal{S}_K(t)$ denote a set of users that are scheduled when K users are selected as an MU-MIMO transmission group at time slot t. The optimal UE group, denoted by $\mathcal{S}^*(t)$, is determined by selecting a set of users that maximize the proportional fairness metric [17] as follows:

$$\mathcal{S}^*(t) = \underset{\mathcal{S}_K(t),\, K \in \{1, 2, \ldots, K_{\max}\}}{\arg\max} \sum_{u \in \mathcal{S}_K(t)} \frac{R_{u|\mathcal{S}_K(t)}}{T_u(t)}, \tag{6}$$

where $R_{u|\mathcal{S}_K(t)}$ denotes the bandwidth efficiency of the uth UE (that is, $R_{u|\mathcal{S}_K(t)} = \log_2(1+\gamma_u)$), γ_u is the SINR of the uth UE for $u \in \mathcal{S}_K(t)$, and $T_u(t)$ denotes the average throughput of the uth UE at time slot t, which is updated for all UE as

$$T_u(t+1) = \begin{cases} (1-1/t_c)T_u(t) + R_{u|\mathcal{S}^*(t)}/t_c & u \in \mathcal{S}^*(t), \\ (1-1/t_c)T_u(t) & u \notin \mathcal{S}^*(t). \end{cases} \tag{7}$$

The parameter t_c in (7) defines time window in which we wish to achieve fairness. We consider dynamic switching between SU-MIMO and MU-MIMO as shown in Fig. 2. SU-MIMO can be regarded as a special case of MU-MIMO with $K = 1$.

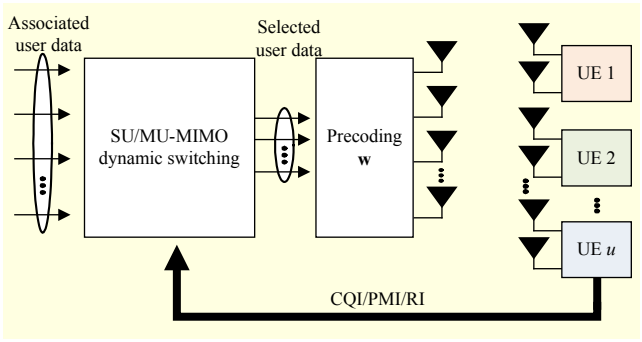

Fig. 2. System model: SU/MU-MIMO dynamic switching.

2. MU-MIMO Feedback Schemes

In an SU-MIMO, each UE selects its own best PMI, which is reported to the eNB along with the CQI corresponding to the selected PMI. In an MU-MIMO system, similarly, UEs shall report some information to the eNB to select the best set of users. Depending on the type of feedback information in this paper, we consider two different feedback schemes for MU-MIMO: a multiuser channel quality information (MU-CQI) scheme [18], [19] and an MUI scheme [13].

A. MU-CQI Feedback Scheme

In the MU-CQI feedback scheme, UEs report the *best companion* PMIs that can be co-scheduled to maximize the SINR in (4). One simple approach that can reduce the feedback overhead is to consider only 2-user MU-MIMO systems; which selects the best companion PMI (q_u, c_u) such that

$$q_u = \underset{i=1, 2, \ldots, |\mathcal{W}|}{\arg\max} \left\|\tilde{\mathbf{H}}_u \mathbf{w}_i\right\|_{\mathrm{F}}^2 \tag{8}$$

and

$$c_u = \underset{i=1, 2, \ldots, |\mathcal{W}|}{\arg\min} \left\|\tilde{\mathbf{H}}_u \mathbf{w}_i\right\|_{\mathrm{F}}^2. \tag{9}$$

Then, the MU-CQI for a given UE u is given by

$$\gamma_u = \frac{\left|\mathbf{g}_u \tilde{\mathbf{H}}_u \mathbf{w}_{q_u}\right|^2}{2\sigma_u^2 + \left|\mathbf{g}_u \tilde{\mathbf{H}}_u \mathbf{w}_{c_u}\right|^2}. \tag{10}$$

Then, UE u reports (q_u, c_u, γ_u) to the eNB, which will be used to determine the best companion PMIs [18]. With this

ETRI Journal, Volume 38, Number 2, April 2016
http://dx.doi.org/10.4218/etrij.16.0115.0064

scheme, the inter-UE interference can be effectively minimized. In this paper, we consider a more aggressive approach to investigate the best possible performance of an MU-CQI scheme for $K_{\max} = 2$. More specially, each UE u reports the PMI q_u, determined by (8), along with a set of CQI for all other PMIs except q_u; that is, $\{(q_u, c_u, \gamma_u)\}_{c_u \in \mathcal{C} \setminus q_u}$. In this way, the eNB can consider all possible UE-pairs for a 2-user MU-MIMO by (6). Furthermore, CQI for SU-MIMO must be also reported to support the dynamic switching between SU-MIMO and MU-MIMO for the system model in Fig. 2. Along with PMI associated with the CB and CQI for the selected PMI, a rank indicator is required to enable a single layer or two layers for SU-MIMO. For a 2-user MU-MIMO system (that is, $K_{\max} = 2$), therefore, a total number of feedback values include one for RI, one for SU-MIMO PMI, one for SU-MIMO CQI, one for MU-MIMO PMI, and $|\mathcal{W}|-1$ for MU-MIMO CQI. As the amount of feedback overhead increases exponentially as K increases, the MU-CQI scheme may not be realistic for $K > 2$.

B. MUI Feedback Scheme

To deal with the feedback overhead problem with the MU-CQI scheme for $K > 2$, [13] considers the MUI feedback scheme, in which each UE u reports the PMI q_u with the best signal-to-noise ratio (SNR), along with the INRs for all other PMIs except q_u, as follows:

$$\mathrm{INR}_{u,c_u} = \frac{\left|\mathbf{g}_u \tilde{\mathbf{H}}_u \mathbf{w}_{c_u}\right|^2}{\sigma_u^2} \qquad (c_u \in \mathcal{C} \setminus q_u). \tag{11}$$

Let $\mathcal{V}$ denote a set of PMIs that are reported by the UE in the scheduled user group $\mathcal{S}$; that is, $\mathcal{V} = \{q_u\}_{u \in \mathcal{S}}$. Since all of the INR feedback information for each UE is known to the eNB, we can rewrite the SINR for UE u as

$$\gamma_u = \frac{\mathrm{SNR}_{u,q_u}}{K + \sum_{i \in \mathcal{V} \setminus q_u} \mathrm{INR}_{u,i}} \qquad (K \in \{1, 2, \ldots, K_{\max}\}), \tag{12}$$

where $\mathrm{SNR}_{u,q_u} = \left|\mathbf{g}_u \tilde{\mathbf{H}}_u \mathbf{w}_{q_u}\right|^2 / \sigma_u^2$. Since each UE u reports its own SNR_{u,q_u} along with a set of INRs, $\{\mathrm{INR}_{u,c_u} | c_u \in \mathcal{C} \setminus q_u\}$, the number of feedback values for the MUI scheme will be $|\mathcal{W}|$ (one for SNR and $|\mathcal{W}|-1$ for INR values). The total number of feedback values will be the same as in the MU-CQI scheme (that is, one for RI, one for SU-MIMO PMI, one for SU-MIMO CQI, one for MU-MIMO PMI, one for SNR, and $|\mathcal{W}|-1$ for INR). Even with the same amount of feedback, however, the MUI feedback scheme allows for K-user grouping as opposed to the MU-CQI feedback scheme, in which only two-user grouping is considered due to its overhead.

Feedback overhead can be further reduced if partial MUI and 1-bit MUI feedback schemes are considered [13]. The partial MUI feedback scheme reports INR for PMIs in one of two subsets defined by $i_1 = 0$ or 1, reducing the feedback overhead by 1/2. Meanwhile, a 1-bit MUI feedback scheme can be implemented by employing a bit map to report the INR values. More specifically, the INR value is set to 1 if it is lower than a given threshold value, which is defined relative to SNR, and to 0 otherwise, significantly reducing its feedback overhead.

III. Simulation Results

This section presents the system-specific simulation results of SU-MIMO and MU-MIMO systems. Our evaluation methodology is strictly based on the simulation scenarios and system model in the 3GPP standardization process. In particular, it implements the 3D channel model in [14], which has been verified by conducting phase-1 and phase-2 channel parameter calibrations with and without a fast-fading mode. Furthermore, the overall SLS has been verified by the baseline throughput calibration specified in [14]. The calibration is completed by referring to the cumulative distribution function (CDF) reported by multiple companies [20].

We follow the simulation parameters for the SLS in [14] and [15], which are summarized in Table 1. While SU-MIMO simulations use nine sub-bands (PUSCH 3-1 format), MU-MIMO (both MU-CQI and MUI schemes) simulations employ wideband feedback to reduce the feedback overhead. For simplicity of the simulation, we use four bits per CQI instead of differential encoding. We assume that only one or two UEs can be supported simultaneously in MU-CQI due to the feedback limit to $K_{\max} = 2$. On the contrary, MUI can simultaneously support a large number of UEs with the same amount of feedback overhead. The maximum number of UEs for MU-MIMO with the MUI feedback scheme is limited to eight (that is, $K_{\max} = 8$) in this simulation. Only fixed tilting is applied to the vertical axis by following the method discussed in [14] and [16], while adaptive beamforming is applied to the horizontal axis using the CB structure discussed in Section II-1-B.

1. System Evaluation Results

In this section, system evaluation results are presented in terms of the spectral efficiency (SE). Figure 3 shows the CDFs of the SE for MU-MIMO in a UMi environment with antenna configurations of (8, 4, 2), (4, 8, 2), and (4, 16, 1). Note that the antenna configurations under consideration are feasible for implementation in real systems. In Fig. 3, there are noticeable gaps in the SE between the MU-CQI ($K_{\max} = 2$) and MUI schemes ($K_{\max} = 8$). Comparing the performance of these schemes with SU-MIMO, the corresponding SE performance

Table 1. Evaluation assumptions.

Parameter		Value
Channel model		3D-UMa (ISD = 500 m), 3D-UMi (ISD = 200 m)
Channel bandwidth		10 MHz
Carrier frequency		2 GHz
Duplexing		FDD
Network layout		Hexagonal grid, 19 cell sites, 3 sectors per site
Wrapping method		Geographical distance-based
Antenna configuration	Tx	(8, 4, 2), (4, 8, 2), (10, 2, 2) : ±45° (4, 16, 1)
	Rx	(1, 1, 2) : 0° and 90°
Polarized antenna model		Model-1 from 3GPP TR36.873 [14]
UE distribution		3D-UMi and 3D-UMa scenarios [14]
UE speed		3 km/h
UE attachment		Based on RSRP [14]
UE array orientation	$\Omega_{UT,\alpha}$	Uniformly distributed on (0, 360°)
	$\Omega_{UT,\beta}$	90°
	$\Omega_{UT,\gamma}$	0°
UE antenna pattern		Isotropic antenna gain pattern $A'(\theta',\phi') = 1$
# of UEs per cell		10
Traffic model		Full buffer
# of layers	SU-MIMO	1 or 2 layers
	MU-MIMO	Up to 8 layers for MUI
Scheduler		Proportional fair scheduling per TTI allocation
Feedback information	SU-MIMO	4 Tx: Rel-8 CB [21], 8 Tx: Rel-10 double CB [22], 16 Tx: double CB for $P = 2$ & DFT CB for $P = 1$
	MU-MIMO	Wideband PMI, CQI, MUI or MU-CQI $P = 1$: oversampled DFT-based CB $P = 2$: subsampled double CB
Feedback type	SU-MIMO	Sub-band feedback
	MU-MIMO	Wideband feedback
Feedback period		5 ms
Receiver		Ideal channel estimation MMSE-IRC receiver
Interference model		Ideal interference estimation from interference measurement resource
Hybrid ARQ		Maximum of 4 transmissions No error on ACK/NACK 8 ms delay between retransmissions
Overhead	DL CCHs	3 symbols
	CRS	16 REs/PRB/subframe
	CSI-RS	Every 5 ms for 4/8/16 port and 1RE/port/ PRB
	DM-RS	12 REs/PRB/subframe

improvements are 10.3% and 24.6%, respectively. It implies that high-order MU-MIMO can substantially improve the system performance over the SU-MIMO system.

Table 2 shows the cell average, median, and lowest 5% SEs of SU-MIMO, MU-CQI, and MUI schemes for an antenna configuration of (8, 4, 2), respectively. Although wideband feedback is used for the MU-MIMO schemes (both MU-CQI and MUI), they outperform that of SU-MIMO, which is based on feedback from nine sub-bands.

Table 3 shows the SEs for an antenna configuration of (4, 8, 2). Owing to the increased spatial separation in horizontal beamforming (recalling that fixed tilting is applied to the vertical axis), a larger performance gain has been achieved, especially for the MU-MIMO schemes. Note that the MUI performance gap between UMi and UMa is larger than that of Table 2. Table 4 shows the SEs for an antenna configuration of (4, 16, 1). Comparing the results against those for (4, 8, 2) in Table 3 (both with the same number of antenna elements), we can see that much larger MU-MIMO performance gain can be achieved with ULA.

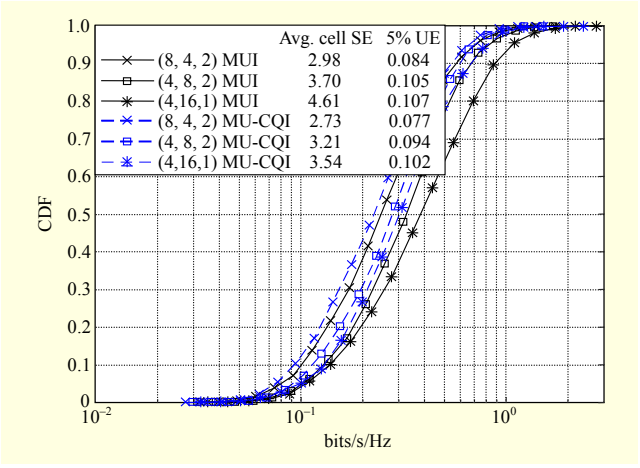

Fig. 3. CDF of MU-MIMO throughput with various antenna configurations: UMi.

Table 2. Evaluation results for (8, 4, 2).

Feedback schemes		Cell average throughput (bps/Hz)	Median UE throughput (bps/Hz)	5% UE throughput (bps/Hz)
PUSCH 3-1 SU-MIMO (baseline)	UMa	2.20 (0%)	0.169 (0%)	0.057 (0%)
	UMi	2.30 (0%)	0.178 (0%)	0.066 (0%)
MUI	UMa	2.72 (24%)	0.230 (36%)	0.084 (48%)
	UMi	3.00 (29%)	0.246 (38%)	0.082 (25%)
MU-CQI ($K = 2$)	UMa	2.64 (20%)	0.225 (33%)	0.077 (36%)
	UMi	2.73 (19%)	0.232 (30%)	0.076 (15%)

ETRI Journal, Volume 38, Number 2, April 2016
http://dx.doi.org/10.4218/etrij.16.0115.0064

Table 3. Evaluation results for (4, 8, 2).

Feedback schemes		Cell average throughput (bps/Hz)	Median UE throughput (bps/Hz)	5% UE throughput (bps/Hz)
PUSCH 3-1 SU-MIMO (baseline)	UMa	2.37 (0%)	0.189 (0%)	0.066 (0%)
	UMi	2.54 (0%)	0.202 (0%)	0.073 (0%)
MUI	UMa	3.42 (44%)	0.277 (46%)	0.098 (49%)
	UMi	3.70 (46%)	0.332 (64%)	0.103 (41%)
MU-CQI ($K=2$)	UMa	2.76 (16%)	0.227 (20%)	0.078 (18%)
	UMi	3.21 (26%)	0.283 (40%)	0.094 (28%)

Table 4. Evaluation results for (4, 16, 1).

Feedback schemes		Cell average throughput (bps/Hz)	Median UE throughput (bps/Hz)	5% UE throughput (bps/Hz)
PUSCH 3-1 SU-MIMO (baseline)	UMa	2.19 (0%)	0.180 (0%)	0.069 (0%)
	UMi	2.45 (0%)	0.209 (0%)	0.079 (0%)
MUI	UMa	3.75 (71%)	0.293 (63%)	0.091 (33%)
	UMi	4.61 (88%)	0.392 (88%)	0.106 (35%)
MU-CQI ($K=2$)	UMa	3.13 (43%)	0.267 (48%)	0.088 (28%)
	UMi	3.54 (44%)	0.302 (44%)	0.100 (27%)

2. Feedback Overhead Reduction Schemes

Table 5 compares the amount of feedback overhead for various schemes. Although the MUI scheme achieves better performance as compared to the MU-CQI scheme with the same amount of feedback overhead (for example, 81 bits), the additional overhead compared to SU-MIMO is significant. For example, a corresponding gain over SU-MIMO requires 2.6 times as many more feedback bits. The additional feedback overhead is not negligible and more practical methods need to be used in real systems. Compared to the MUI scheme, both the partial MUI scheme and the 1-bit MUI scheme can reduce the feedback overhead by 40% (for example, 49 bits) and 56% (for example, 36 bits), respectively. Note that the 1-bit MUI scheme incurs only 16% more feedback overhead than the SU-MIMO. The INR threshold in the 1-bit MUI scheme is a critical parameter for the system performance and must be carefully determined. To achieve an acceptable performance, the SNR-based adaptive threshold shown in Fig. 4 is used for the simulations rather than using the fixed threshold in [13].

Table 6 shows the SEs of the partial MUI and 1-bit MUI schemes as compared to the MUI scheme. Note that their performances do not significantly degrade (around 10% or less in most cases) while they substantially reduce the feedback overhead.

Table 5. Wideband MU-MIMO feedback overhead comparison ($T=9$, $O=15$ co-PMIs, offset level $B=4$).

Feedback schemes	RI	PMI	CQI	MU-CQI	MUI	Total
PUSCH 3-1 SU-MIMO (baseline)	1	$8=4$(1st) $+4$(2nd)	$4+2T$	N/A	N/A	31 bits
MUI	1	$8+4$	$4+4$	N/A	$B\cdot O$	81 bits
Partial MUI	1	$8+4$	$4+4$	N/A	$\frac{B(O-1)}{2}$	49 bits
1-bit MUI	1	$8+4$	$4+4$	N/A	O	36 bits
MU-CQI (K=2)	1	$8+4$	$4+4$	$B\cdot O$	N/A	81 bits
MU-CQI (K=3)	1	$8+4$	$4+4$	$O\sum_{j=1}^{K-1}\binom{L}{j}$	N/A	501 bits

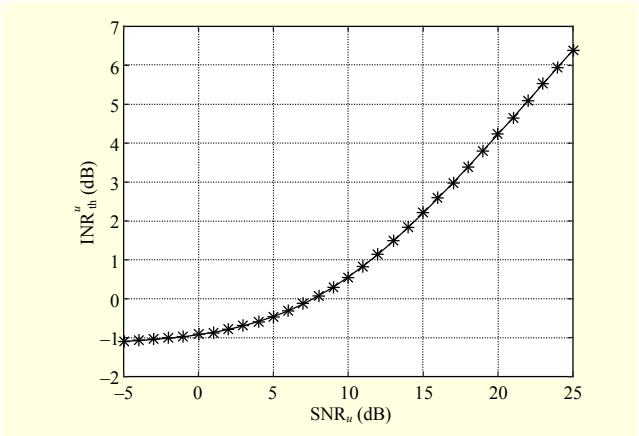

Fig. 4. INR threshold for 1-bit MUI scheme.

The $|\mathcal{W}|$ values of CQI feedback are required for the MUI scheme (more specifically, 1 SNR value and $|\mathcal{W}|-1$ INR values). Figure 5 illustrates the CDFs for 31 values of INR, given by (10), for one specific (but typical) UE for the different oversampled values i_1, where $i_1 = 0$ or 1 in this simulation. Depending on the value of i_1, there exist two groups of INR values. While all INR values (32 values) need to be reported in the MUI scheme, only one group (16 values) is required for feedback in the partial MUI scheme. From Fig. 5, we can see that high and low INR values can be easily distinguished even in a single group. This implies that MU-MIMO is feasible with the reduced feedback overhead schemes (for example, the partial MUI scheme or the 1-bit MUI scheme). However, high-order MU-MIMO is less probable with the partial MUI or 1-bit MUI schemes, since the candidate UEs of simultaneous transmissions will be limited as compared to the MUI scheme. Figure 6 shows the transmission layer probability in a UMi environment with an antenna configuration of (4, 16, 1). We

Table 6. Performance attenuation with feedback reduction.

Feedback schemes			Cell average throughput (bps/Hz)	Median UE throughput (bps/Hz)	5% UE throughput (bps/Hz)
(8, 4, 2)	MUI	UMa	2.72 (0%)	0.230 (0%)	0.084 (0%)
		UMi	3.00 (0%)	0.246 (0%)	0.082 (0%)
	Partial MUI	UMa	2.59 (–5%)	0.212 (–8%)	0.074 (–12%)
		UMi	2.80 (–6%)	0.223 (–9%)	0.072 (–13%)
	1-bit MUI	UMa	2.56 (–6%)	0.216 (–6%)	0.074 (–11%)
		UMi	2.73 (–8%)	0.228 (–7%)	0.086 (5%)
(4, 8, 2)	MUI	UMa	3.42 (0%)	0.277 (0%)	0.098 (0%)
		UMi	3.70 (0%)	0.332 (0%)	0.103 (0%)
	Partial MUI	UMa	3.08 (–10%)	0.251 (–9%)	0.086 (–13%)
		UMi	3.65 (–1%)	0.311 (–6%)	0.111 (8%)
	1-bit MUI	UMa	2.97 (–13%)	0.247 (–11%)	0.082 (–17%)
		UMi	3.25 (–12%)	0.280 (–16%)	0.097 (–6%)
(4, 16, 1)	MUI	UMa	3.75 (0%)	0.293 (0%)	0.091 (0%)
		UMi	4.61 (0%)	0.392 (0%)	0.106 (0%)
	Partial MUI	UMa	3.69 (–2%)	0.298 (2%)	0.092 (1%)
		UMi	4.18 (–10%)	0.361 (–8%)	0.103 (–2%)
	1-bit MUI	UMa	3.43 (–9%)	0.287 (–2%)	0.095 (4%)
		UMi	3.66 (–21%)	0.317 (–19%)	0.101 (–5%)

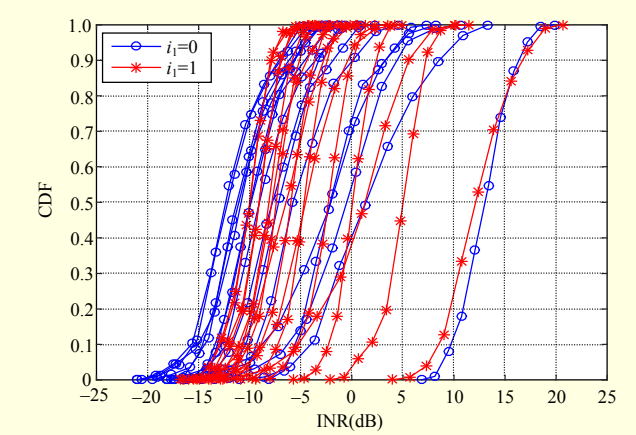

Fig. 5. CDF of INR with CB: UMi and (4, 16, 1).

can see that the performance is significantly degraded with the feedback reduction schemes, especially when the order of MU-MIMO increases; for example, $K \geq 6$.

IV. Further Analysis with Various System Configurations

In addition to the previous simulation results on the overall system performance, we provide additional results to analyze how SU-MIMO and MU-MIMO performances are respectively governed by the different antenna configurations and channel environments. The current analysis will provide an insightful basis for understanding the system-level performance. The same simulation parameters and scenarios as in Section III are considered for the further analysis.

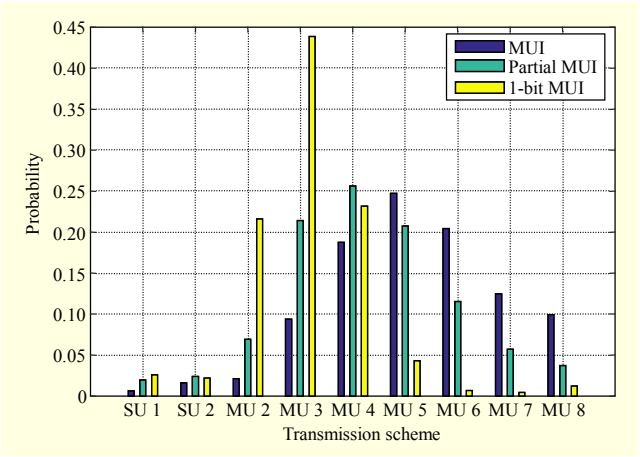

Fig. 6. Probability of transmission schemes with different numbers of layers: UMi and (4, 16, 1).

1. Antenna Configurations: X-pol vs. ULA

Figure 7 presents the 2D beam patterns for the different antenna configurations, (4, 16, 1) and (4, 8, 2), with the same number of antenna elements. Figures 7(a) and 7(b) show the beam gain pattern for azimuth angle of 30°, beamformed with DFT codebook, and elevation beam pattern for 102° tilting, respectively. It is obvious that the different antenna arrangement induces the different beam pattern, even if the same number of antennas is employed. In particular, the beam pattern of (4, 16, 1) is narrower than that of (4, 8, 2). Our simulation results are also consistent with both the current observation and the field measurement data for FD-MIMO in [3]. For the SU-MIMO, meanwhile, it has been shown that the average throughput with (4, 8, 2) is higher than that with (4, 16, 1). This is attributed to the fact that more spatial multiplexing gain can be achieved with X-pol, which involves less correlation between polarization signals. However, a narrow beam pattern of the ULA might be more useful to high-order MU-MIMO, as will be shown in Figs. 8 and 9.

The channel capacity is affected not only by the maximal singular value of the channel, denoted as $\lambda_{\max}$, but also by its minimal value, denoted as $\lambda_{\min}$. We can define their ratio as the *condition number*; that is, $\lambda_{\max}/\lambda_{\min}$. The lower the condition number (that is, a well-conditioned channel), the greater the capacity, since a low correlation is involved in providing higher spatial multiplexing gain [23]. Figure 8 shows

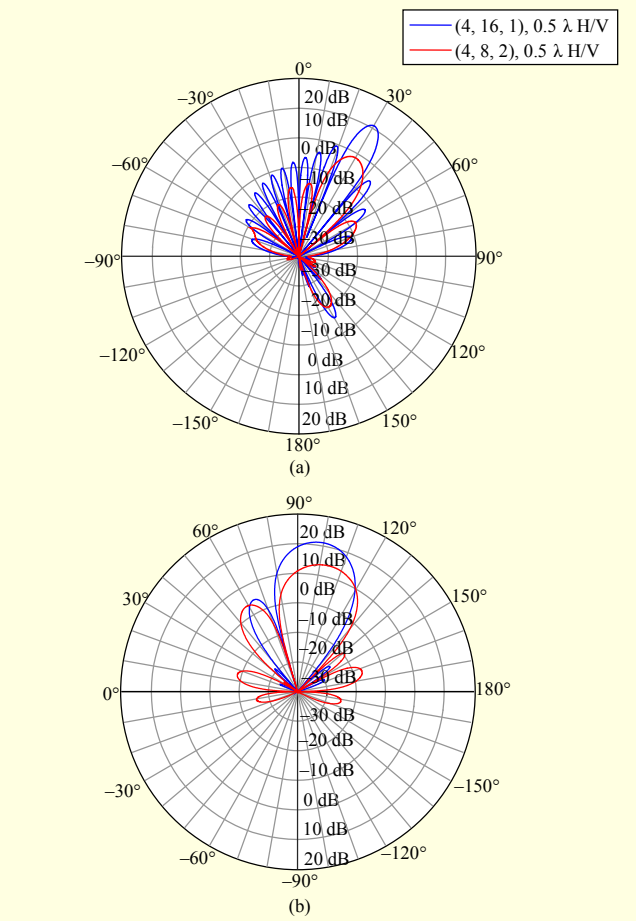

Fig. 7. Beam gain patterns with fixed azimuth angle (30°) and fixed vertical tilting angle (102°): (a) azimuth and (b) elevation.

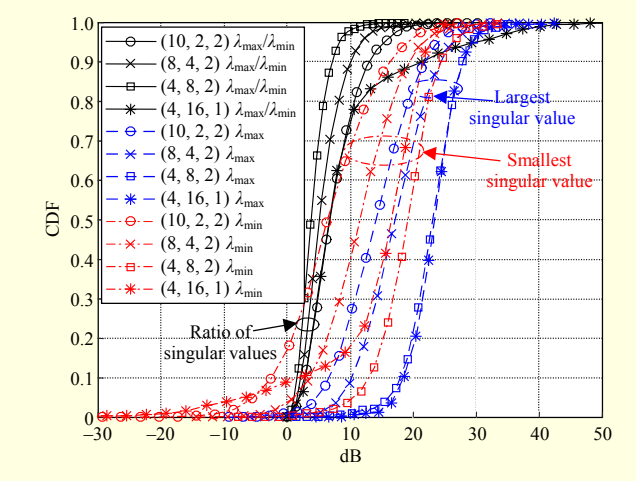

Fig. 8. Singular values with various antenna configurations.

the condition numbers for the different antenna configurations, including the one for (10, 2, 2) reported by Phase-2 calibration in [14]. Furthermore, a CDF of the baseline throughput is presented in Fig. 9. It is observed that X-pol (10, 2, 2) and (8, 4, 2) are well-conditioned as opposed to the ULA. In particular, 20% of users are ill-conditioned for the ULA. The advantage of X-pol antennas is attributed to the additional dimension obtained by cross polarization. Meanwhile, λ_{max} increases with N, which improves a beam gain.

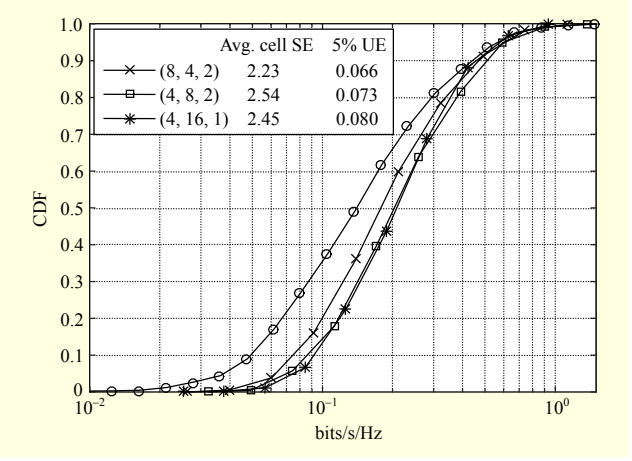

Fig. 9. CDF of baseline throughput: UMi.

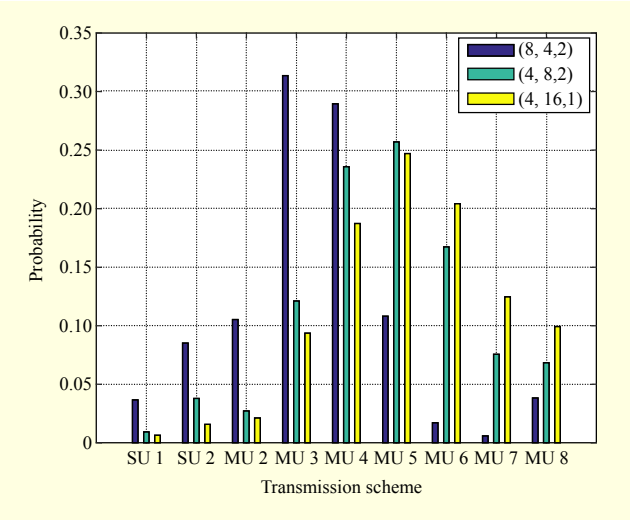

Fig. 10. Probabilities of transmission schemes with different numbers of layers: UMi.

Note that the average cell-SE is mainly governed by the spatial multiplexing gain, while the beamforming gain is attributed to the cell-edge SE. In fact, it is clear that the average cell-SE of (4, 8, 2) is greater than that of (4, 16, 1), while 5% UE SE of (4, 16, 1) is greater than that of (4, 8, 2).

Figure 10 shows the probabilities of various transmission schemes with different numbers of transmission layers, where the SU-MIMO and MU-MIMO schemes are dynamically switched by scheduling. It is observed that a group of three or four users are selected for MU-MMO mostly when the antenna configuration of (8, 4, 2) is used, while a group of four, five, or six users are selected frequently for (4, 16, 1) and (4, 8, 2),

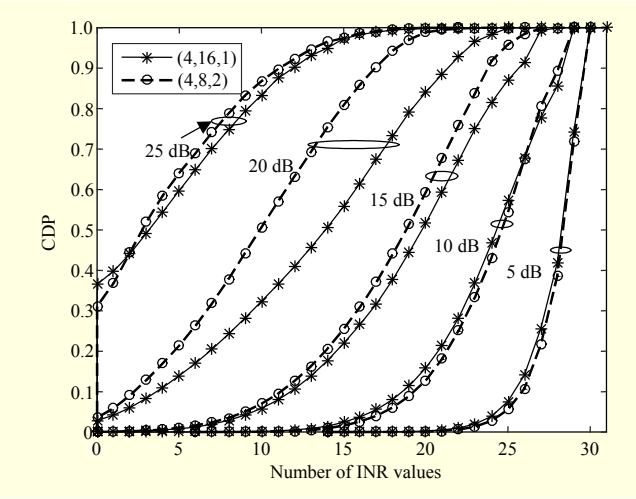

Fig. 11. CDF of number of INRs that satisfy given SNR-INR gap: UMi.

realizing the narrower beams. It is clear that ULA (4, 16, 1) is more useful to high-order MU-MIMO than X-pol (4, 8, 2).

For the antenna configurations of (4, 16, 1) and (4, 8, 2), each UE will report one SNR value and 31 INR values to the eNB, in which the SINR can be computed by (11). Those INR values that are of a significant distance from the SNR will make good-companion PMIs. Figure 11 shows a CDF for the number of INRs that corresponds to good-companion PMIs subject to the given SNR-INR gap or better. It is obvious that the number of good-companion PMIs increases as the required SNR-INR gap decreases. We find that the two antenna configurations (4, 16, 1) and (4, 8, 2) show a significant difference in the number of INRs that provide good-companion PMIs when the SNR-INR gap is subject to 20 dB or better. This observation leads to a difference in group size of high-order MU-MIMO, which is consistent with the results in Fig. 10. For example, since a greater number of candidate PMIs are available with ULA (4, 16, 1) than X-pol (4, 8, 2), ULA tends to achieve a higher SE.

2. Environmental Scenarios: Indoor vs. Outdoor and Line-of-Sight vs. Non-line-of-Sight

We consider various channel characteristics in different environments: outdoor line-of-sight (O-LOS), outdoor non-line-of-sight (O-NLOS), indoor LOS (I-LOS), and indoor NLOS (I-NLOS). We consider two different types of channel environments — UMa and UMi — each with different characteristics of LOS, as given by the distribution in Fig. 12. It is observed that LOS is more probable for the UMi environment in which the distance between a UE and the eNB is shorter than that in UMa.

We have demonstrated in Section III-2 that higher throughput

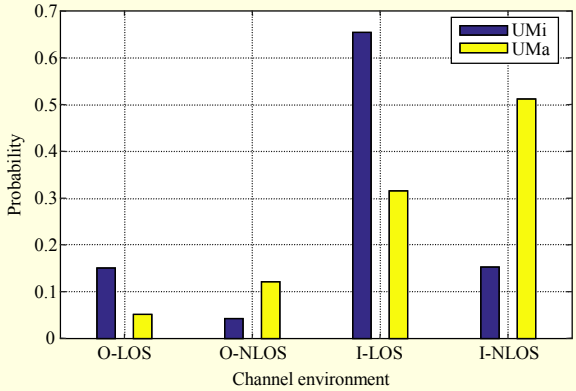

Fig. 12. Channel environments of UE.

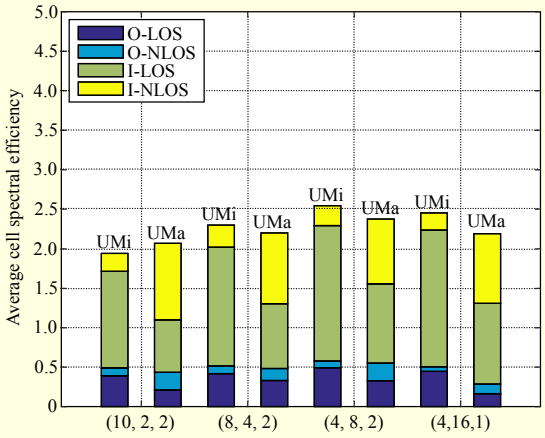

Fig. 13. Average cell spectral efficiency: SU-MIMO.

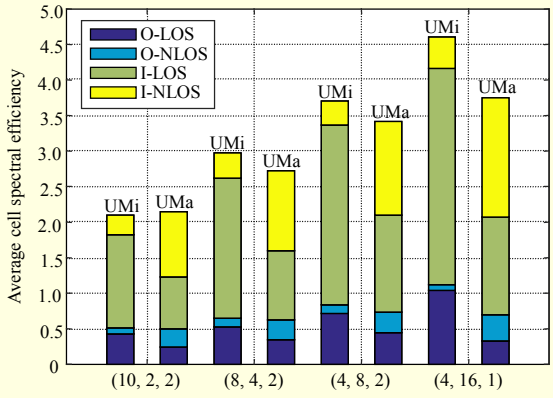

Fig. 14. Average cell spectral efficiency: MU-MIMO.

can be achieved in UMi than UMa as long as the same number of UEs is assumed in each cell; furthermore, the throughput gain for UMi becomes more significant for the MU-MIMO. We first investigate the performance of the SU- MIMO for different channel environments with varying antenna configurations. As shown in Fig. 13, there is not much difference in average cell-SE with the different environments

ETRI Journal, Volume 38, Number 2, April 2016
http://dx.doi.org/10.4218/etrij.16.0115.0064

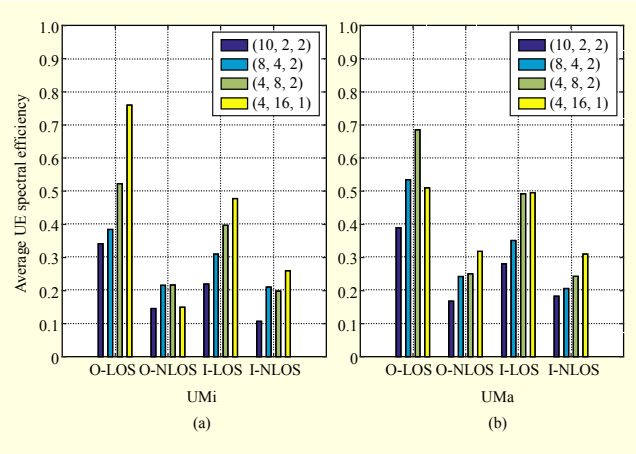

Fig. 15. Average UE spectral efficiency with LOS/NLOS.

and furthermore, even with the various antenna configurations. This is attributed to the fact that the performance of the SU-MIMO is mainly governed by the number of receive antennas and its performance is already saturated by the two receive antennas in the current system.

Figure 14 presents the performance of the MU-MIMO. It is observed that more gain can be achieved in UMi than UMa, simply because UMi finds more LOS UEs, which provide more beam gain or narrow beam patterns, subsequently improving the MU-MIMO gain. Figure 15 confirms the fact that most of the high-throughput UEs belong to O-LOS while many of the low-throughput UEs belong to O-NLOS. In particular, there is a significant gap between UMi and UMa with ULA (4, 16, 1), since LOS UEs in UMi are significantly improved by ULA narrow beam patterns.

V. Conclusion

In this paper, we have investigated the system-level performance of an INR-based MU-MIMO feedback scheme (MUI) for a massive MIMO system, especially under the standard 3D channel model (specified by 3GPP TR36.873). Our SLS results have demonstrated that the MUI scheme is acceptable for supporting the high-order MU-MIMO, as opposed to the existing MU-CQI scheme, which is typically limited to two-user grouping only. Furthermore, it has been shown that the performance of the high-order MU-MIMO can be improved with a ULA configuration, in which the beam patterns are very narrow compared to X-pol, and in a UMi environment, in which LOS UEs are dominant compared to a UMa environment. Meanwhile, we have investigated the possibility of reducing feedback overhead for an MUI without compromising the performance gain. In particular, the 1-bit MUI schemes can reduce the feedback overhead by 50% while incurring only 10% performance degradation. However, the overall gain still varies with the antenna configurations and channel environments. In our future work, further optimization of a feedback scheme will be performed, and a more effective feedback overhead reduction scheme will be developed for high-order MU-MIMO system.

References

[1] T.L. Marzetta, "Noncooperative Cellular Wireless with Unlimited Numbers of Base Station Antennas," *IEEE Trans. Wireless Commun.*, vol. 9, no. 11, Nov. 2010, pp. 3590–3600.

[2] E.G. Larsson et al., "Massive MIMO for Next-Generation Wireless Systems," *IEEE Commun. Mag.*, vol. 52, no. 2, Feb. 2014, pp. 186–195.

[3] Y. Kim et al., "Full Dimension MIMO: The Next Evolution of MIMO in LTE Systems," *IEEE Wireless Commun.*, vol. 21, no. 2, Apr. 2014, pp. 26–33.

[4] N. Jindal, "MIMO Broadcast Channels with Finite Rate Feedback," *IEEE Trans. Inf. Theory*, vol. 52, no. 11, Nov. 2006, pp. 5045–5060.

[5] J. Choi et al., "Noncoherent Trellis Coded Quantization: A Practical Limited Feedback Technique for Massive MIMO Systems," *IEEE Trans. Commun.*, vol. 61, no. 12, Dec. 2013, pp. 5016–5029.

[6] A. Adhikary et al., "Joint Spatial Division and Multiplexing - the Large-Scale Array Regime," *IEEE Trans. Inf. Theory*, vol. 59, no. 10, Oct. 2013, pp. 6441–6463.

[7] J. Nam et al., "Joint Spatial Division and Multiplexing: Opportunistic Beamforming, User Grouping and Simplified Downlink Scheduling," *IEEE J. Sel. Topics Signal Process.*, vol. 8, no. 5, Oct. 2014, pp. 876–890.

[8] A. Adhikary et al., "Joint Spatial Division and Multiplexing for mm-Wave Channels," *IEEE J. Sel. Areas Commun.*, vol. 32, no. 6, June 2014, pp. 1239–1255.

[9] Y. Xu, G. Yue, and S. Mao, "User Grouping for Massive MIMO in FDD Systems: New Design Methods and Analysis," *IEEE Access*, vol. 2, Sept. 2014, pp. 947–959.

[10] X. Rao and V.K.N. Lau, "Distributed Compressive CSIT Estimation and Feedback for FDD Multiuser Massive MIMO Systems," *IEEE Trans. Signal Process.*, vol. 62, no. 12, June 2014, pp. 3261–3271.

[11] J. Choi, D.J. Love, and P. Bidigare, "Downlink Training Techniques for FDD Massive MIMO Systems: Open-Loop and Closed-Loop Training with Memory," *IEEE J. Sel. Topics Signal Process.*, vol. 8, no. 5, Oct. 2014, pp. 802–814.

[12] J. Nam et al., "On the Role of Transmit Correlation Diversity in Multiuser MIMO Systems," Preprint, submitted to *IEEE Trans. Inf. Theory*, arXiv:1505.02896, 2015.

[13] J. Nam, "Doubly Opportunistic Beamforming," Preprint, submitted to *IEEE Trans. Inf. Theory*, 2015.

[14] 3GPP TR 36.873 V12.0.0, *Study on 3D Channel Model for LTE*, Release 12, Sept. 2014.
[15] 3GPP TR 36.897 V0.1.1, *Study on Elevation Beamforming/Full-Dimension (FD) MIMO for LTE*, Release 13, Nov. 2014.
[16] A. Kammoun et al., "Preliminary Results on 3D Channel Modeling: From Theory to Standardization," *IEEE J. Sel. Areas Commun.*, vol. 32, no. 6, June 2014, pp. 1219–1229.
[17] M. Kountouris and D. Gesbert, "Memory-Based Opportunistic Multiuser Beamforming," in *Proc. IEEE Int. Symp. Inf. Theory*, Adelaide, Australia, Sept. 4–9, 2005, pp. 1426–1430.
[18] Y. Du et al., "Evaluation of PMI Feedback Schemes for MU-MIMO Pairing," *IEEE Syst. J.*, vol. 4, no. 4, 2010, pp. 505–510.
[19] Y. Dai et al., "A PMI Feedback Scheme for Downlink Multiuser MIMO Based on Dual-Codebook of LTE-Advanced," in *Proc. IEEE Veh. Tech. Conf.*, Quebec City, Canada, Sept. 2012, pp. 1–5.
[20] R1–143469, "*Summary of 3D Channel Model Calibration Results*," Nokia Networks, Nokia Corporation, RAN1#78, 2014.
[21] 3GPP TS 36.211, *Evolved Universal Terrestrial Radio Access (EUTRA); Physical Channels and Modulation*, Release 12, 2014.
[22] 3GPP TS 36.213, *Evolved Universal Terrestrial Radio Access (EUTRA); Physical Layer Procedures*, Release 12, 2014.
[23] T.S. Rappaport, "*Wireless Communications: Principles and Practices*," 2nd ed., Upper Saddle River, NJ, USA: Prentice Hall, 2002.

Yongin Choi received his BS degree in electrical engineering from Korea University, Seoul, Rep. of Korea, in 2010. Since then, he has been with the Department of Electrical Engineering, Korea University, partaking in a combined MS and PhD course. His research interests include radio resource management; multiple-input and multiple-output communication systems; and cross-layer design for mobile radio communication systems and wireless networks.

Jaewon Lee received his BS degree in information and communication engineering from Chungbuk National University, Cheongju, Rep. of Korea, in 2014. Since then, he has been with the Department of Telecommunication System Technology, Korea University, Seoul, Rep. of Korea, partaking in a combined MS and PhD course. His research interests include massive MIMO and waveforms.

Minjoong Rim received his BS degree in electronics engineering from Seoul National University, Rep. of Korea, in 1987 and his PhD degree in electrical and computer engineering from the University of Wisconsin, Madison, USA, in 1993. From 1993 to 2000, he worked for Samsung Electronics, Seoul, Rep. of Korea. Currently, he is a professor at Dongguk University, Seoul, Rep. of Korea. His research interests include mobile and wireless communications.

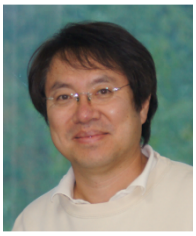

Chung Gu Kang received his BS degree in electrical engineering from the University of California, San Diego, USA, in 1987 and his MS and PhD degrees in electrical & computer engineering from the University of California, Irvine, USA, in 1989 and 1993, respectively. Since March 1994, he has been with both the Department of Radio Communication & Engineering and the Department of Electrical Engineering, Korea University, Seoul, Rep. of Korea, where he is currently a full professor. He is currently serving on the "5G Forum of Korea" — a private and public cooperative platform for globally leading and promoting 5G technologies — as a chair of the subcommittee for wireless technology. His research interests include broadband wireless transmission technologies; radio access technologies for massive connectivity and low latency in cellular IoT infrastructure; and cross-layer design for mobile systems.

Junyoung Nam received his BS degree in statistics from Inha University, Incheon, Rep. of Korea, in 1997 and his MS and PhD degrees in electrical engineering from KAIST, Daejeon, Rep. of Korea, in 2008 and 2015, respectively. He was with the Communications R&D Center, Samsung Electronics, Seoul, Rep. of Korea, from 1997 to 2002. He was also with the Communications Lab., Seodu InChip, Seoul, Rep. of Korea, from 2002 to 2006. In 2006, he joined ETRI. His research interests include wireless communications, information theory, and 5G system design.

Young-Jo Ko received his BS, MS, and PhD degrees in physics from KAIST, Daejeon, Rep. of Korea, in 1992, 1994, and 1998, respectively. He is currently a director of Wireless Transmission Research Section 1 of the Wireless Transmission Research Department, ETRI. He joined ETRI in 1998 and has been working on mobile communications. His current research interests include LTE evolution and 5G enabling technologies, particularly focusing on wireless transmission and aspects of the physical layer.